Climate Dynamics (2019) 53:895–905
https://doi.org/10.1007/s00382-019-04624-4

NAO implicated as a predictor of the surface air temperature multidecadal variability over East Asia

Tiejun Xie[1] · Jianping Li[1,2] · Cheng Sun[1] · Ruiqiang Ding[3] · Kaicun Wang[1] · Chuanfeng Zhao[1] · Juan Feng[1]

Received: 13 September 2018 / Accepted: 8 January 2019 / Published online: 14 January 2019

Abstract
Surface air temperature is an important factor for human quality of life and is a key marker of global climate change. Understanding multidecadal changes in surface air temperature, and accurately predicting future trends, are therefore important for economic development. In this work, we explore multidecadal variability in East Asian surface air temperature (EASAT). We find that EASAT shows a strong multidecadal variability between 1900 and 2017. Observational analysis shows that annual EASAT multidecadal variability is highly associated with the North Atlantic oscillation (NAO) and the NAO leads detrended annual EASAT by 15–20 years. Further analysis illustrates that the NAO precedes annual EASAT multidecadal variability through its leading effect on the Atlantic Multidecadal oscillation (AMO). The AMO influences annual EASAT multidecadal variability through the Africa–Asia multidecadal teleconnection (AAMT) pattern. An NAO-based linear model is therefore established to predict annual EASAT. The model is able to better hindcast annual EASAT based on different periods of the time-series. Due to the joint influences of NAO multidecadal variability and the forcing associated with anthropogenic greenhouse gas emissions, annual EASAT for 2018–2034 is predicted to remain at its current level or even slightly lower, followed by a period of fast warming over the following decades.

Keywords East Asian surface air temperature · North Atlantic oscillation · Atlantic multidecadal oscillation · Africa–Asia multidecadal teleconnection pattern

1 Introduction

East Asia (20°–40°N, 90°–120°E) is a highly populated area and one of major agricultural, industrial and economic centers of the world. To the west of East Asia lies the world's highest plateau, the Tibet Plateau, and to the east the Pacific Ocean, the largest ocean in the world. The climate system in East Asia is complex and it plays an important role in global climate change (Zhang and Liu 1992; Zhou et al. 2004). Multidecadal climate change, particularly multidecadal temperature change, is closely related to the long-term economic and social development of a region and to the lives of its population (Yoshino 1978; Robeson et al. 2014; Lin and Franzke 2015; Stolpe et al. 2017). Recognizing the mechanisms behind multidecadal temperature change and effectively predicting temperature change over the coming decades provides an important reference for governments to formulate a strategy for tackling climate change (Stolpe et al. 2017). The Intergovernmental Panel on Climate Change (IPCC) has made multidecadal climate change and its prediction one of the core elements of its assessment report (Taylor et al. 2012), and the IPCC AR5 (Fifth Assessment Report) also attaches importance to research on and prediction of multidecadal trends (Stocker et al. 2014).

As in many other regions of the world, annual East Asian surface air temperature (EASAT) increased markedly during the twentieth century and shows characteristics of multidecadal change (Levitus et al. 2001; Ding et al. 2007; Luo and Li 2014). Unlike the continuously rapid warming of EASAT between 1985 and 2005, over recent years the areal-averaged

✉ Jianping Li
ljp@bnu.edu.cn

[1] College of Global Change and Earth System Sciences (GCESS), Beijing Normal University, Beijing 100875, China

[2] Laboratory for Regional Oceanography and Numerical Modeling, Qingdao National Laboratory for Marine Science and Technology, Qingdao 266237, China

[3] State Key Laboratory of Numerical Modeling for Atmospheric Sciences and Geophysical Fluid Dynamics (LASG), Institute of Atmospheric Physics, Chinese Academy of Sciences, Beijing 100029, China

annual EASAT is not obviously increased, perhaps indicative of a warming hiatus (Fig. 1a). This feature warrants further investigation. The impact of natural climate phenomena such as the Atlantic Multidecadal oscillation (AMO) (Luo and Li 2014; Kucharski et al. 2016; Stolpe et al. 2017; Sun et al. 2018; Li et al. 2018a), the Atlantic meridional overturning circulation (AMOC) (Sun et al. 2012; Stolpe et al. 2018), the Pacific Decadal oscillation (PDO) (Liu et al. 2006; Luo and Li 2014; Stolpe et al. 2017), the El Niño–Southern oscillation (ENSO) (Bradley et al. 1987; Hu et al. 2012), and the Indian Ocean Dipole (IOD) (Guan and Yamagata 2003; Zhao et al. 2014), together with the impact of human activities (Hua et al. 2008; Li et al. 2016, 2018b) such as the heat island effect, the effect of greenhouse gas emissions, and the impact of aerosols on climate change within East Asia has been investigated in previous studies. However, the mechanism of EASAT multidecadal variability has not been fully understood.

Future changes to East Asian temperatures have been explored using climate model simulations (Ding et al. 2007; Wang and Chen 2014; Yang et al. 2017) and theoretical model prediction (Luo and Li 2014). Surface air temperature (SAT) consistently shows a warming trend under different CO_2 emission scenarios for different regions in East Asia, but with rates differing between climate models (Wang and Chen 2014; Yang et al. 2017). However, few climate models are able to simulate the recent warming hiatus over East Asia (Meehl et al. 2014; Meehl and Teng 2014). According to the statistical relationship between annual EASAT multidecadal internal variability and the sea surface temperature (SST) mode, Luo and Li (2014) developed an extrapolation approach to predicting annual EASAT based on the AMO's quasiperiodicity. However, as changes to the SST mode in the future may not be completely regular, use of the interdecadal SST mode to predict annual EASAT has limitations (Luo and Li 2014). Therefore, to explore future changes in annual EASAT, a new model is needed.

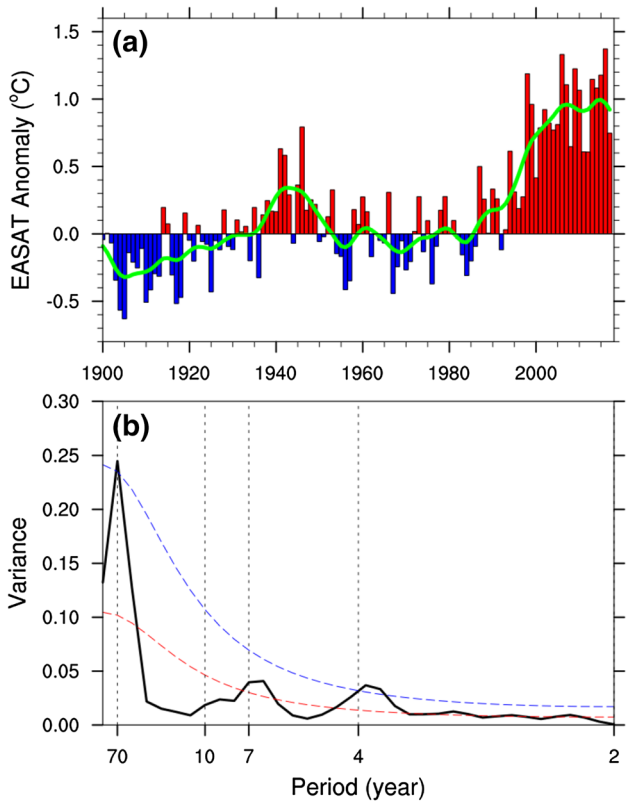

Fig. 1 Time series of annual EASAT anomalies, and power spectrum. **a** Areal-averaged annual EASAT anomalies (bars) for the period 1900–2017, based on the HadCRUT4 dataset and relative to the base period 1961–1990. The solid green line is annual EASAT anomalies after Gaussian low-pass filtering. **b** Power spectrum of annual EASAT anomalies for the period 1900–2017. The blue and red dashed lines show the 95% confidence level and the reference red noise spectrum, respectively

The North Atlantic oscillation (NAO) is the dominant mode of atmospheric variability over the North Atlantic region (Walker 1924; Wallace and Gutzler 1981; Hurrell 1995; Li and Wang 2003; Sun et al. 2015; Wang et al. 2017) and fluctuates on timescales ranging from interannual to multidecadal (Luterbacher et al. 1999; Polyakov and Johnson 2000; Wanner et al. 2001). The study of the NAO is a key target of the International Climate Variability and Predictability Program (CLIVAR) (WCRP 2018). Based on analysis of the atmospheric circulation in the Northern Hemisphere, it has been found that the NAO is not only a regional phenomenon (Li and Wang 2003; Hurrell 1996; Hurrell et al. 2003; Li et al. 2013; Yu et al. 2016). The NAO can affect the climate system over East Asia via teleconnections and anomalous stationary waves (Chen et al. 2005; Li and Ruan 2018) through two branches (Hoskins 1993; Zuo et al. 2015): the northern branch, oriented along the subpolar waveguide (Chen et al. 2005; Gong et al. 2001; Wu and Wang 2002), and the southern branch of the wave train, which propagates from the North Atlantic southeastward into Europe and the Arabian Gulf via the Asian jet waveguide (Zuo et al. 2015; Bueh et al. 2011). However, these studies are more focused on the synoptic timescale, and there are few studies on multidecadal temperature changes over East Asia affected by the NAO. Based on observational analysis, Li et al. (2013) showed that the NAO leads Northern Hemisphere mean surface temperature by 15–20 years, and therefore concluded that the NAO is a predictor of Northern Hemisphere mean surface temperature (Li et al. 2013). These results provide an incentive for studying the effects of the NAO on multidecadal variations in annual EASAT.

In this paper, we explore the relationship between the NAO and annual EASAT on the multidecadal scale using observations and theoretical analysis. We find that NAO has a leading effect on the annual EASAT on the multidecadal scale and is a predictor of the annual EASAT. An AMO

bridge mechanism is identified to explain that by which the NAO affects multidecadal variability in the annual EASAT. An NAO-based linear model is therefore established to predict annual EASAT. We have performed hindcast on this model to test the uncertainty of the model. Finally, annual EASAT for 2018–2034 is predicted.

2 Data and methodology

2.1 Data

The NAO index (NAOI) was calculated from NCAR SLP (National Center for Atmospheric Research Sea Level Pressure) observational data (Trenberth and Paolino 1980) at a horizontal (latitude–longitude) resolution of 5°×5° for the period 1899–2017, obtained from the US National Center for Environmental Prediction. In addition, we used HadSLP2 (Hadley Centre Sea Level Pressure dataset 2) (Allan and Ansell 2006) at a resolution of 5°×5° from the UK Met Office Hadley Center and the Climatic Research Unit at the University of East Anglia, which covers the period 1850–2017. As the results of this study were not sensitive to the choice of dataset for sea level pressure, we show only results obtained using NCAR SLP data. SAT observational data include observations from 160 stations in China covering 1951–2017 and the China SAT 0.5°×0.5° gridded dataset (V2.0) for 1961–2017; HadCRUT4 (version 4 of the Institute of Climate of the University of East Anglia, UK) data (Morice et al. 2012), which combine land and sea surface temperature datasets from the UK Met Office Hadley Center and the Climatic Research Unit at the University of East Anglia, at a horizontal resolution of 5°×5° and covering the period 1850–2017; and GISTEMP (GISS Surface Temperature) (Hansen et al. 2010) covering 1880–2017 from NASA's Goddard Institute for Space Studies (GISS). In exploring the relationship between the NAO and annual EASAT, comparing results obtained using these datasets, noting that the results are not sensitive to the choice of dataset, we have only shown results obtained using HadCRUT4 data. In terms of the mechanism of annual EASAT change, the lack of HadCRUT4 data for central North Africa mans that we used the High Precision Surface Climate Data Set (CRU TS 4.01) (University of East Anglia Climatic Research Unit 2017) of the University of East Anglia Institute of Climatology at a horizontal resolution of 0.5°×0.5° for 1901–2016. For wind and geopotential height data we used Twentieth Century Reanalysis Version 2 (20CRv2) data (Compo et al. 2011) from the US National Oceanic and Atmospheric Administration (NOAA), which are at a resolution of 2°×2° and covering the period 1871–2012.

Based on data availability, the historical simulations data from 40 Atmosphere–Ocean General Circulation Models (ACCESS1-0, ACCESS1-3, BCC-CSM1-1, BCC-CSM1-1-m, BNU-ESM, CanESM2, CCSM4, CESM1-BG, CESM1-CAM5, CESM1-FASTCHEM, CESM1-WACCM, CMCC-CESM, CMCC-CM, CMCC-CMS, CNRM-CM5, CSIRO-Mk3-6-0, EC-EARTH, FGOALS-g2, FGOALS-s2, GFDL-CM3, GFDL-ESM2G, GFDL-ESM2M, GISS-E2-H, GISS-E2-R, HadCM3, HadGEM2-ES, INM-CM4, IPSL-CM5A-LR, IPSL-CM5A-MR, IPSL-CM5B-LR, MIROC-ESM, MIROC-ESM-CHEM, MIROC5, MPI-ESM-LR, MPI-ESM-MR, MPI-ESM-P, MRI-CGCM3, MRI-ESM1, NorESM1-M, NorESM1-ME) that participated in CMIP5 were used to further verify the relationship between NAO and EASAT. Monthly output for the period 1900–2005 from historical simulations based upon the first realization (r1i1p1) of all models (except EC-EARTH, for which r7i1p1 is used due to data availability) is considered.

2.2 Statistical method

In this paper, NAOI is defined as the difference between the normalized zonal mean sea level pressure in the region between the middle latitudes (35°N) and the high latitudes (65°N) of the North Atlantic (80°W–30°E) (Li and Wang 2003). Both in observations (Hilmer and Jung 2000) and in some model future projections (Hu and Wu 2004), the active centers of NAO have spatial shift. Such shift may influence the NAOI definition. In view of this, this definition has been compared to another definition based on the principal component (PC) time series of the leading empirical orthogonal function decomposition (EOF) of annual sea surface pressure (SLP) anomalies over the Atlantic sector (20°–80°N, 90°W–40°E) (Hurrell 1995; Hurrell et al. 2003). The results are not sensitive to the choice of NAOI definition, therefore we have only shown results based on the definition of Li and Wang (2003). Annual EASAT is defined as the area-weighted mean SAT of the East Asia region (20°–40°N, 90°–120°E). The AMO index is defined as the area-weighted mean SST anomaly of the North Atlantic (0°–60°N, 7.5°–75°W). In exploring the multidecadal teleconnection with the Asian jet stream, the Africa–Asia multidecadal teleconnection (AAMT) index is defined as follows:

$$\mathrm{AAMT} = \frac{1}{6}\left[\left(V_1^*+V_3^*+V_5^*\right) - \left(V_2^*+V_4^*+V_6^*\right)\right],$$

where V_1^*, V_2^*, V_3^*, V_4^*, V_5^* and V_6^* are the standardized 300 hPa meridional wind anomalies for the regional average of A_1 [18°–26°N, 48°–40°W], A_2 [18°–26°N, 4°W–4°E], A_3 [22°–30°N, 14°–22°E], A_4 [20°–28°N, 48°–56°E], A_5 [18°–26°N, 86°–94°E] and A_6 [20°–28°N, 110°–118°E], respectively.

We used a two-tailed *t* test to assess statistical significance. The number of degrees of freedom is the number of

effective degrees of freedom. In the case of significance tests for the correlation coefficient between two variables with high autocorrelation, especially for time series after low-pass filtering, the number of degrees of freedom for the sample is taken as the number of effective degrees of freedom. The number of effective degrees of freedom (N^{eff}) is calculated as follows (Pyper and Peterman 1998; Li et al. 2013):

$$\frac{1}{\mathrm{N}^{\text{eff}}} \approx \frac{1}{\mathrm{N}} + \frac{2}{\mathrm{N}} \sum_{j=1}^{N} \frac{N-j}{\mathrm{N}} \rho_{XX}(j)\rho_{YY}(j),$$

where N is the sample size and $\rho_{XX}(j)$ and $\rho_{YY}(j)$ are the autocorrelations of two sampled time series X and Y at time lag j, respectively.

This study employs statistical methods, including power spectrum analysis, Gaussian low-pass filtering, correlation analysis, and linear regression, which are not described in detail here.

3 Multidecadal variations in annual EASAT and relationship to NAO

Since the beginning of the twentieth century, annual EASAT has shown a trend of warming with fluctuations and multidecadal variations, similar to the change in global temperature. Annual EASAT was in a cold phase during 1900–1930 and 1953–1987, and in a warm phase during 1930–1953 and from 1990 to the present day derived from the HadCRUT4 data (Fig. 1a). Annual EASAT showed a trend of fluctuating warming between 1900 and around 1945. Annual EASAT reached a maximum around 1945, and since then has shown a gradual cooling, although with fluctuations. From 1955 to around 1990, annual EASAT remained relatively stable with only small fluctuations. From 1990 until 2010, there was a clear trend of rapid and fluctuating warming, rising at a rate of 0.2 °C every 10 years, which is higher than the rate of global ground-based temperature increase over the same period (Hansen et al. 2006). From 2010 to recent years, the annual EASAT was not obviously increased. This multidecadal feature is clearly demonstrated using continuous power spectrum analysis (Fig. 1b). Observed annual EASAT shows a significant spectral peak at a period of ~ 70 years. In addition, there are peaks over quasi-decadal scales at ~ 7 years and interannual scales at ~ 4 years. The statistical significance of the multidecadal variation should be interpreted carefully, as the analysis period covers only one and a half cycles of annual EASAT. Nevertheless, a multidecadal variability of 50–70 years has been reported in several studies based on observed and reconstructed annual EASAT time series (Gao et al. 2015). The reason for the change in annual EASAT may be external forcing due to anthropogenic factors such as increased emission greenhouse gases (including carbon dioxide), while multidecadal fluctuations may reflect a change in internal variability.

Both NAOI and annual EASAT anomalies show multidecadal variability, with NAOI generally leading the phase of annual EASAT by 10–20 years, where NAOI derived from NCAR SLP data (Fig. 2a). From 1900, NAOI increased to its maximum value, before decreasing below zero until it reached its minimum value, before increasing gradually. According to this behavior, the index has a period of 50–70 years, consistent with previous studies (e.g., Schlesinger 1994). NAOI was in a clear positive phase between roughly 1900 and 1935, and between 1970 and 2005, and in its negative phase between roughly 1935 and 1970. Annual EASAT also shows obvious characteristics of multidecadal variability. Annual EASAT gradually increased from the start of the twentieth century, peaking around 1943, before falling to its lowest value between 1970 and 1980, and then gradually increasing. Between 2005 and 2010, it reached its maximum value, before dropping slightly in recent years. Annual EASAT was in a positive phase between 1900 and 1955 and from 1995 to present day, and in a negative phase

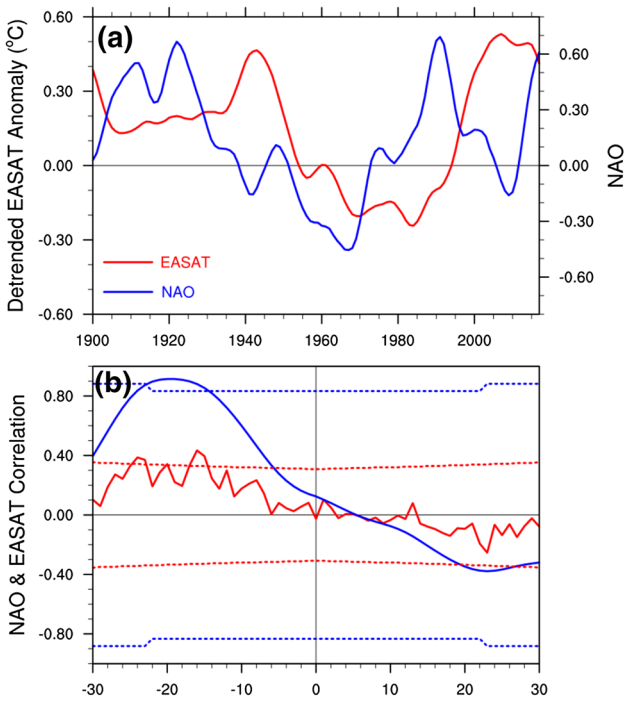

Fig. 2 EASAT, NAOI, and their lead–lag correlation. **a** Detrended annual EASAT anomalies (red line) and NAOI (blue line) from 1900 to 2017 after Gaussian low-pass filtering. **b** Lead–lag correlation between annual mean NAOI and detrended annual EASAT anomalies (1900–2017). The red (blue) line is for the annual mean (Gaussian low-pass filtered) time series. Negative (positive) lags mean that the NAOI leads (lags) detrended annual EASAT, and the red (blue) dashed lines denote the 98% confidence levels for unfiltered (filtered) time series using the effective number of degrees of freedom

between 1955 and 1995. The change in annual EASAT is in good agreement with the change in NAOI, with a leading period of 10–20 years. These results suggest that annual mean NAOI precedes annual EASAT, and therefore that NAOI can be implicated as a predictor of multidecadal variability in annual EASAT.

To further explore the relationship between NAO and annual EASAT, we assess the lead–lag correlation between annual mean NAOI and detrended annual EASAT (Fig. 2b). For the unfiltered time series, the correlation coefficient reaches a maximum value of 0.45 (significant above the 98% confidence level) when NAOI leads detrended annual EASAT by around 15–17 years. For the filtered time series, the correlation coefficient reaches its maximum value of 0.91 (significant above the 98% confidence level) when NAOI leads annual EASAT by 17 years. This result illustrates that NAO potentially has a sizeable impact on SAT over East Asia and may be a predictor of multidecadal variability in annual EASAT. Meanwhile, this relationship consistent among different SLP datasets such as HadSLP2 (not shown). Thus, these results further suggest that the observed NAO–EASAT connection is robust.

For East Asia, Gaussian low-pass filtered NAOI with a lead time of 17 years correlates well with SAT based on Gaussian low-pass filtered HadCRUT4 data (Fig. 3a). Almost the entire region has a lead correlation coefficient exceeding 0.6, with the value exceeding 0.8 for many areas and passing the 98% significance level (*t* test). Results are similar using SAT data from 160 Chinese stations or China's SAT 0.5° × 0.5° gridded dataset. This further illustrates that multidecadal variability in annual EASAT is related to the NAO.

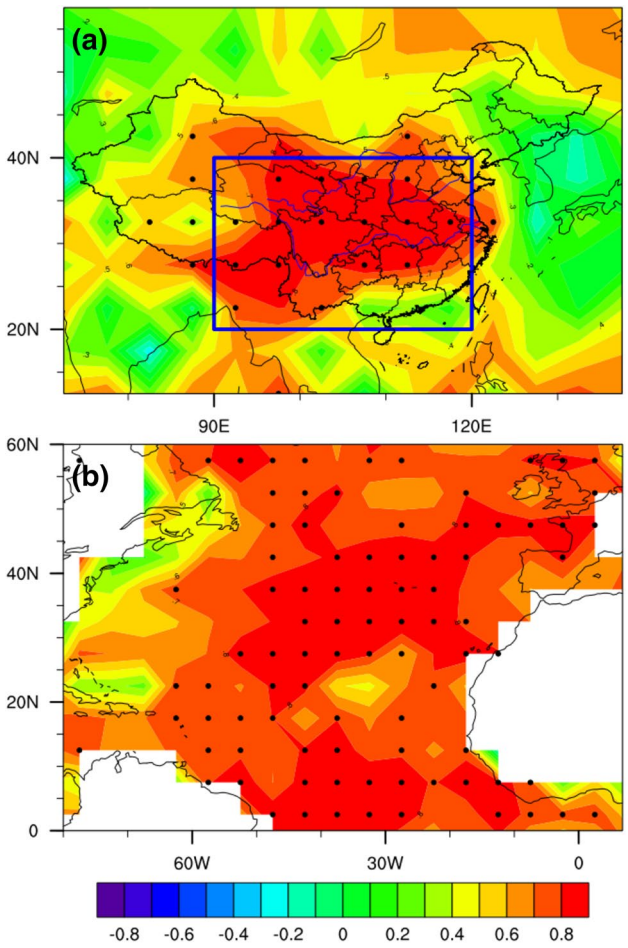

Fig. 3 Lead correlation between NAO, SAT, and SST. **a** Lead correlation between annual NAOI during 1900–2000 and detrended annual SAT over East Asia during 1917–2017 based on Gaussian low-pass filtered data. The dotted area denotes correlations significant above the 95% confidence level. The blue box indicates the East Asian region considered in this study (20°−40°N, 90°−120°E). **b** As in (**a**) but for SST anomalies over the North Atlantic

4 Mechanism by which NAO influences multidecadal variability in annual EASAT

It remains unclear how the NAO affects annual EASAT with a phase lag of 17 years. Sun et al. (2015, 2017) proposed the NAO delay oscillator model and the cold-season North Africa–East Asia teleconnection (Sun et al. 2015, 2017). We found that multidecadal teleconnections exist not only in the cold season but throughout the whole year. In view of the great thermal capacity and thermal inertia of the ocean (Hunt and Wells 1979; Thompson and Schneider 1979; Cess and Goldenberg 1981; Sun et al. 2017) and the existence of the teleconnection, we propose that the NAO affects annual EASAT by storing signals in the ocean. Firstly, the NAO drives deep ocean convection through anomalous turbulent heat fluxes, which in turn affect the AMOC. The AMOC gives rise to AMO-type SST anomalies (Sun et al. 2015, 2017; Stolpe et al. 2018). Then, the AMO affects annual EASAT through the westerly waves of the Northern Hemisphere.

The NAO has a large impact on North Atlantic SST (Peng 2002; Slonosky and Yiou 2002; Scaife et al. 2005; Sun et al. 2015). There is a strong correlation between the NAO and SST variability in the North Atlantic when the NAO leads by 17 years (Fig. 3b); the correlation coefficient exceeds 0.6 over most of the ocean, and exceeds 0.8 in many regions (significant above the 95% confidence level). This correlation arises because the NAO stores signals in the North Atlantic Ocean by acting on the AMOC and then affects the SST of the North Atlantic, with the AMO reflecting the SST variability in this region. This process takes 15–20 years (Li et al. 2013).

It can be seen that AMO index and EASAT almost reached the maximum lead–lag correlation in the same

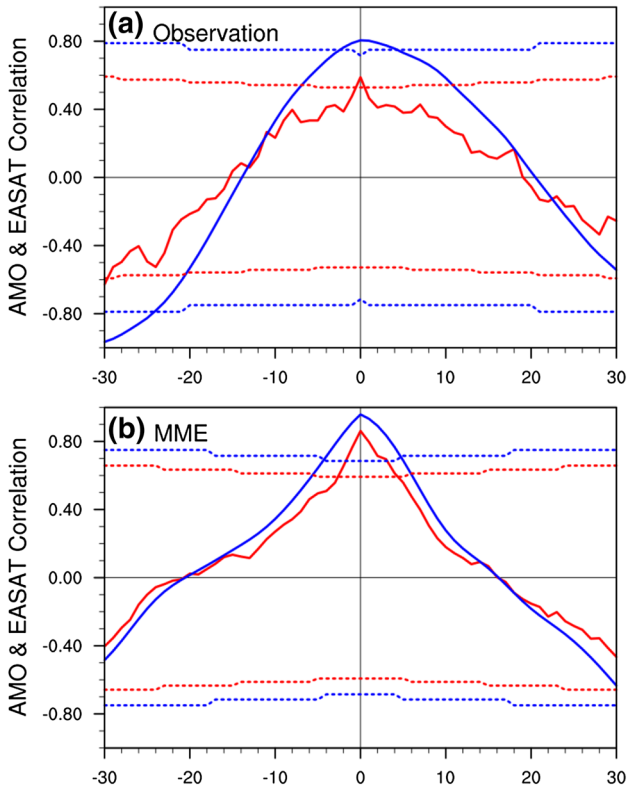

Fig. 4 Lead–lag correlation between AMO and EASAT derived from observations as well as MME. **a** Lead–lag correlation between annual mean AMO index and detrended annual EASAT anomalies (1900–2017). The red (blue) line is for the annual mean (Gaussian low-pass filtered) time series. Negative (positive) lags mean that the AMO index leads (lags) EASAT, and the red (blue) dashed lines denote the 90% confidence levels for unfiltered (filtered) time series using the effective number of degrees of freedom. **b** As in (**a**) but derived from the MME of 17 CMIP5 historical simulations covering the period 1900–2005

period, with a correlation coefficient is 0.81 (Fig. 4a). The lead–lag correlation between AMO index and EASAT (Fig. 4b) based on the multimodel ensemble mean (MME) of 17 CMIP5 historical simulations (ACCESS1-0, ACCESS1-3, BCC-CSM1-1-m, CanESM2, CCSM4, CESM1-CAM5, CMCC-CM, CMCC-CMS, GFDL-CM3, GFDL-ESM2G, HadGEM2-ES, IPSL-CM5A-MR, IPSL-CM5B-LR, MIROC-ESM, MPI-ESM-MR, MRI-CGCM3, and MRI-ESM1) that can better simulate the relationship between AMO and EASAT, reproducing a significant maximum correlation coefficient (0.96) when the AMO index and the EASAT in in-phase, further verify the link between AMO and EASAT.

The AMO index is strongly correlated with the land SAT of regions adjacent to the Mediterranean Sea, the Arabian Peninsula, and the East Asian region, all of which lie between 30°W to 150°E and 10°N to 50°N (Fig. 5). Areas of highest correlation seem to be clustered around 30°N; e.g., northwestern North Africa, Northern Arabia, and East Asia. These three large centers coincide with the westerly wave train. Similar results are obtained using different datasets in place of CRU TS 4.01 (not shown). Therefore, we conclude that the AMO affects SAT in East Asia via the westerly wave train.

The regression method was used to decompose the meridional wind anomaly at 300 hPa in Eurasia (0–60°N, 30°W–150°E). Figure 6a shows the spatial pattern of the Gaussian low-pass filtered V300 anomalies across the Eurasian continent. The spatial pattern is characterized by a zonal wave structure with alternate centers of southerly and northerly anomalies extending from the northwest coast of Africa to East Asia. In North Africa–East Asia between 20°N and 40°N, two positive and three negative centers appear along the 30°N latitude circle, corresponding to a dimension of about 5–6 wavenumbers, as Sun et al. (2017) calculated

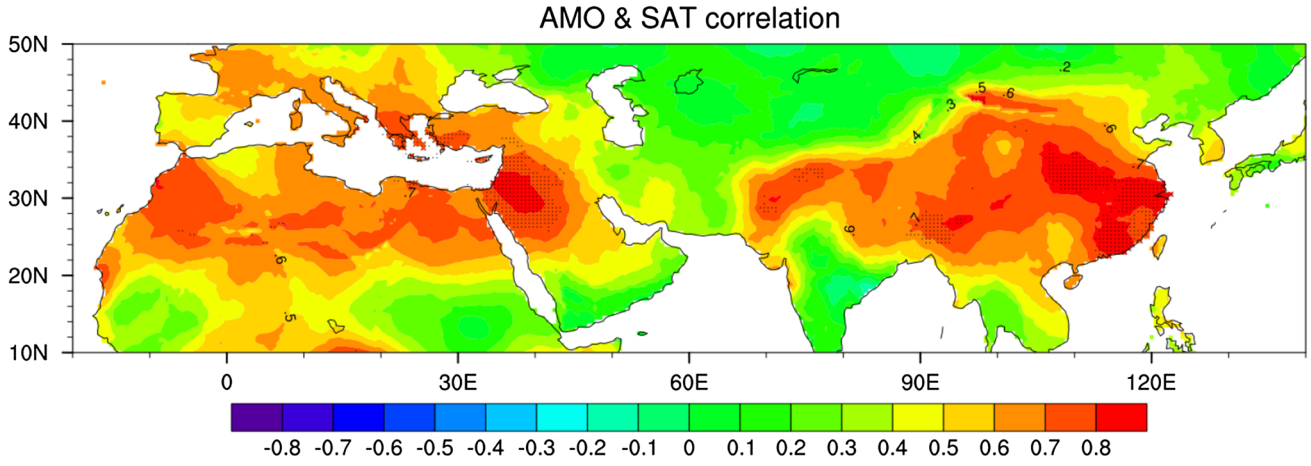

Fig. 5 Correlation map between the Gaussian low-pass filtered annual time series of land SAT and the AMO index between 1901 and 2016. The dotted area denotes correlations significant at the 95% confidence level using the effective number of degrees of freedom

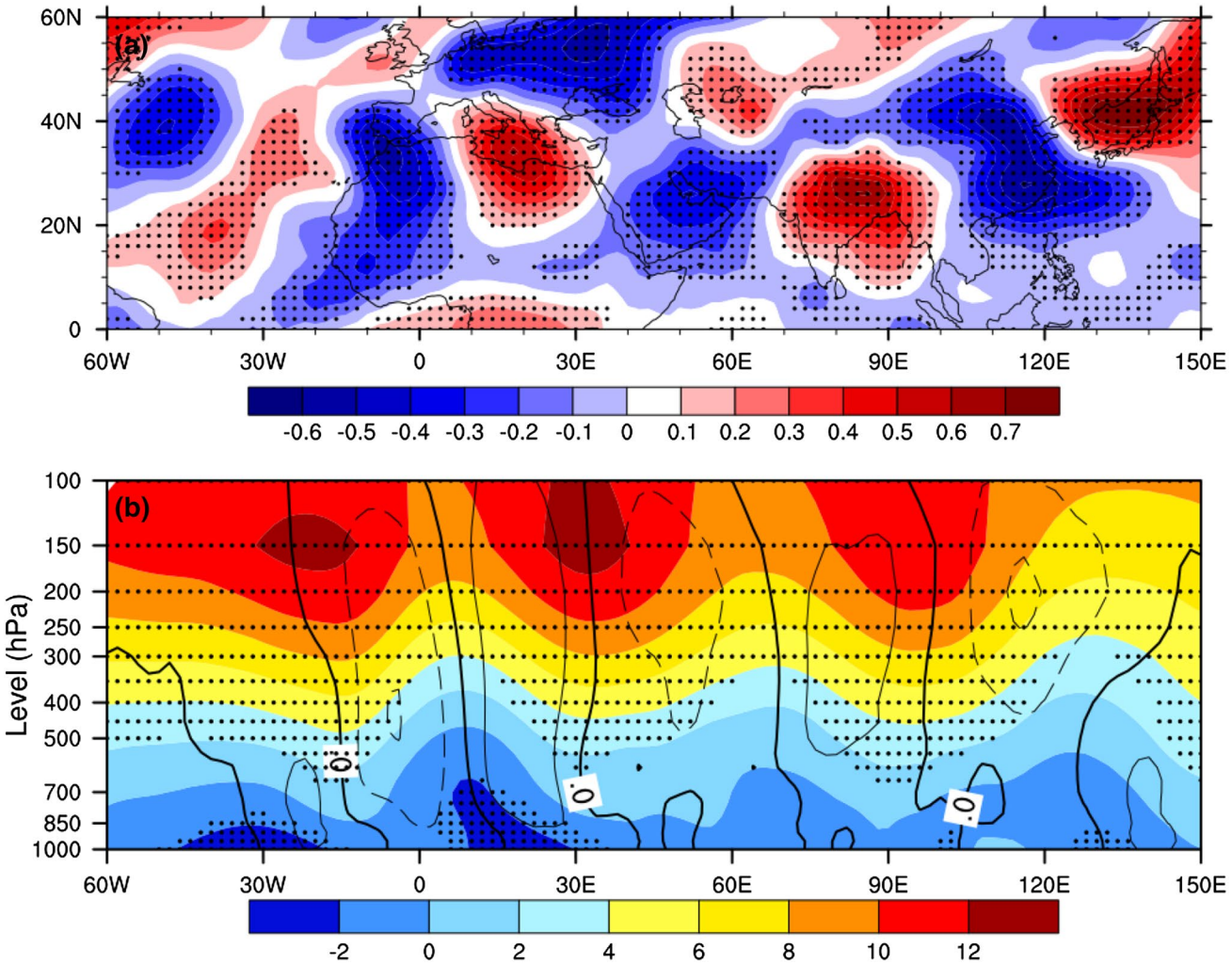

Fig. 6 V300 and geopotential height anomalies regressed onto the AAMT index. **a** Spatial pattern of the Gaussian low-pass filtered annual V300 anomalies over the Eurasian continent (0°–60°N, 60°W–150°E) from 1900 to 2012. The pattern is displayed as V300 ($m{\cdot}s^{-1}$) regressions onto the normalized annual AAMT index. Dots indicate regressions significant above the 99% confidence level using the effective number of degrees of freedom. **b** Annual meridional wind (contours, $m{\cdot}s^{-1}$) and geopotential height anomalies (shading, m) at 25°–35°N regressed onto the normalized annual AAMT index at decadal timescales from 1900 to 2012. Dots indicate the regressions for height are significant above the 95% level, using the effective number of degrees of freedom

using the Rossby wave ray tracing theory in a horizontally nonuniform background flow (Li and Li 2012; Li et al. 2015; Zhao et al. 2015, 2018) in the area from the northwest coast of Africa to East Asia. This shows that the AMO affects EASAT through westerly waves.

To investigate the vertical structure of the AAMT pattern, we calculated the latitudinal averages of meridional wind and geopotential height at 25°–35°N regressed onto the AAMT index over decadal timescales (Fig. 6b). The meridional wind anomalies associated with the AAMT show equivalent barotropic structure in the troposphere with maxima located in the upper troposphere. The geopotential height field shows three centers of maximum positive anomalies in the upper troposphere extending from the northwest coast of Africa to East Asia, with minimum anomalies in between. These positive height anomalies tend to intensify the climatological ridge over Europe but weaken the East Asian trough. The locations of the maxima and minima of the regressed geopotential height anomalies correspond to the zero-value contours of the meridional wind anomalies and are consistent with the geostrophic wind relationship. This shows that the AAMT has a clear vertical structure.

Based on these findings, we propose the NAO first stores signals in the North Atlantic and then influences annual EASAT on the multidecadal scale via the AAMT, which is a very important path that NAO affects EASAT.

5 Multidecadal prediction of annual EASAT

This lead–lag relationship of the NAO and annual EASAT (i.e., with a phase lag of 17 years) offers a simple but useful way to predict annual EASAT around a decade and half in advance. A NAO-based linear model for predicting decadal annual EASAT is therefore established as follows:

$$\mathrm{EASAT}(t) = a\mathrm{NAO}(t\text{-}17) + bt + c,$$

where t is time in years and the coefficients a, b, and c are determined empirically by linear regression based on the data over the historical period, so that the root mean square error of the results from the model and the observations is minimized.

To test the performance of the model, we performed many hindcast experiments. The empirical model used for each hindcast was constructed with only knowledge of the training data before the hindcast period. For example, to hindcast the multidecadal change in the annual EASAT from 2008 to 2024, we constructed model only based on the historical data from 1900 to 2007, in which the parameters a, b, and c are 0.64, 0.010, −19.44, respectively. Similarity, to hindcast the change from 2009 to 2025, we constructed model only based on the historical data from 1900 to 2008, in which the parameters a, b, and c are 0.63, 0.010, −19.27, respectively. These parameters have slight differences between two models constructed based on different periods, but these parameters are quite stable in many hindcast experiments. Some hindcast examples are given in Fig. 7. Such as in Fig. 7a, we set up the model based on historical data from 1900 to 1985, and predicted the multidecadal change in the annual EASAT from 1986 to 2002. Compared with the observed annual EASAT, the hindcast annual EASAT are similar and all in the allowed uncertainty range. Same as in Fig. 7b–d, only based on different period of 1900–1990, 1900–1995 and 1900–2000, to hindcast the annual EASAT of 1991–2007, 1996–2012 and 2001–2017, high correlations and relatively small root mean square errors between the hindcast and observed annual EASAT are obtained for each set of hindcast experiments. Therefore, the model can be used to accurately simulate the multidecadal variation in annual EASAT.

We constructed a model of multidecadal variability in annual EASAT based on data for NAOI (1900–2000) and

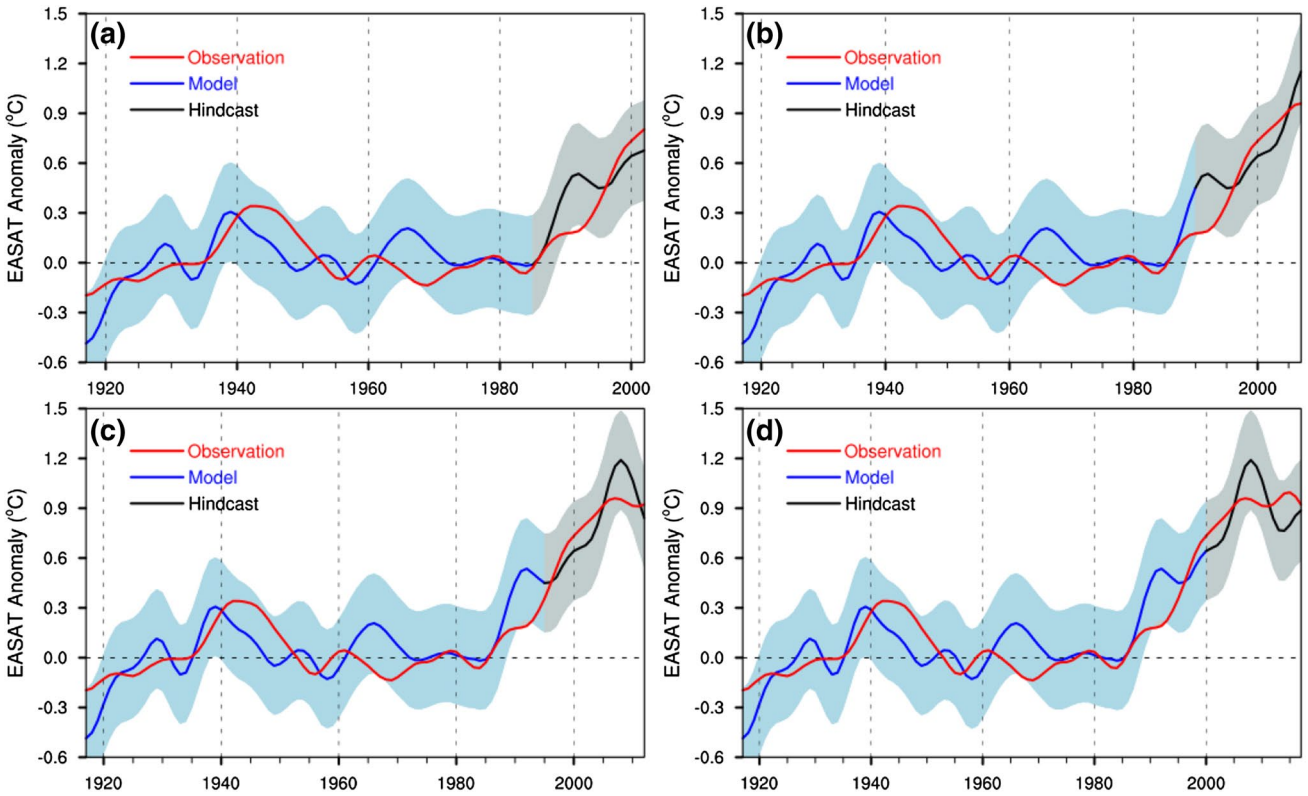

Fig. 7 Observed, modeled, and hindcasted EASAT. **a** Observed annual EASAT (red) after Gaussian low-pass filtering for 1917 to 2002, model predicted annual EASAT (blue) for 1917 to 1985, and hindcasted annual EASAT (black) for 1986–2002. The shaded areas show the 2-sigma uncertainty range of the model predicted and hindcasted values. **b–d** As in (**a**) but for Observed annual EASAT for 1917 to 2007, 2012 and 2017, model predicted annual EASAT for 1917 to 1990, 1995 and 2000, and hindcasted annual EASAT for 1991–2007, 1996–2012 and 2001–2017

annual EASAT (1917–2017). Time series for annual EASAT obtained from observations and from the model predictions are compared in Fig. 8. Gaussian low-pass filtered observed annual EASAT shows a gradual increase from 1917, peaking around 1945. It then decreases slightly and remains steady until 1980 when it begins to gradually increase at a rate exceeding 0.3 °C every 10 years, before entering a warming hiatus around 2010. The model predicted annual EASAT anomaly also rose gradually from 1917, peaking just before 1940, and remained generally steady before entering a period of pronounced warming. In recent years, annual EASAT shows a warming hiatus, in good agreement with observations. The model successfully predicts the two local maxima of annual EASAT around 1940 and 2010, simulates the temperature trends during 1917–1940 and 1980–2010, and predicts the relatively stable annual EASAT between 1940 and 1980. The warming hiatus in annual EASAT over recent years is also well simulated. Observed values are generally within the range of the uncertainty of the model.

Next, we set up the model based on historical data from 1900 to 2017 and predicted the multidecadal change in the annual EASAT from 2018 to 2034 (Fig. 8). The annual EASAT will remain steady at its current level or even slightly lower in coming years due to the weakening of the previous NAO if the external force changes little, and thereafter continues to fast warm based on recent NAO decadal strengthening.

6 Summary and discussion

We used HadCRUT4 surface temperature data to explore the relationship between annual EASAT and the NAO. Annual EASAT and NAOI show clear multidecadal variations. On the multidecadal scale, the phase change of NAOI leads changes in EASAT by 10–20 years. The highest lead–lag correlation for NAOI and EASAT is obtained when NAOI leads EASAT by 17 years; this value is significant above the 98% confidence level (two-tailed *t* test). We therefore conclude that a link exists between NAO and annual EASAT.

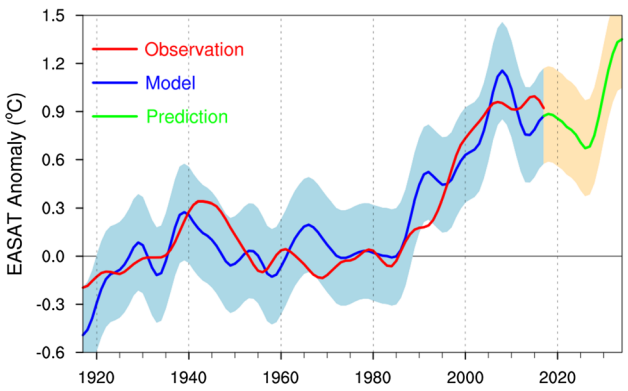

Fig. 8 Observed, modeled, and predicted EASAT. Observed annual EASAT (red) after Gaussian low-pass filtering for 1917–2017, model predicted annual EASAT (blue) for 1917–2017, and predicted annual EASAT (green) for 2018–2034. The shaded areas show the 2-sigma uncertainty range of the model predicted values

Based on the NAO delay oscillator model (Sun et al. 2015, 2017), and considering the great thermal capacity and thermal inertia of the ocean, we propose that the ocean acts as a "bridge" through which the NAO affects annual EASAT. Firstly, NAO drives deep ocean convection through anomalous turbulent heat fluxes, which in turn affect AMOC. The AMO then gives rise to AMO-type SST anomalies that affect annual EASAT via the westerly waves of the Northern Hemisphere. A clear relationship exists between NAO and SST variability in the AMO region. When the NAO leads SST variability by 17 years, there is a large, significant lead–lag correlation between SST and NAOI throughout almost the entire AMO region. To explore the effect of AMO on annual EASAT, we assessed the relationship between the AMO and surface temperature in the North Africa–East Asia region, revealing that the AMO has a strong correlation with SAT in Northwestern Africa, the Arabian Peninsula, and East Asia. To study the mechanisms involved, we explored the African–Asian multidecadal teleconnection AAMT in the North Africa–East Asia region. The regression method was used to decompose the meridional wind anomaly at 300 hPa in Eurasia. Its spatial pattern presents a zonal wave structure with the center extending from Northwest Africa to East Asia. Between 20°N and 40°N, along the 30°N latitude circle, there are two positive and three negative centers in the area from the northwest coast of Africa to East Asia. Based on the regression coefficients obtained from the geopotential height anomalies and the meridional wind anomalies regressed onto the AAMT index, the AAMT is also evident in the vertical direction, confirming the presence of the AAMT and the viability of the proposed mechanism by which NAO affects annual EASAT through the "bridge" effect of the AMO. These above corresponding arguments indicate that the chain of NAO–AMO–AAMT–EASAT is a very important path that NAO affects EASAT.

A multidecadal model of annual EASAT was constructed and used to obtain hindcasts. The predictions were in good agreement with observational data. High correlations and relatively small root mean square errors between the hindcast and observed annual EASAT are obtained for each set of hindcast experiments, indicating that the model can be used to accurately simulate the multidecadal variation in annual EASAT. Finally, based on this linear model, we predicted multidecadal variations in annual EASAT over the next decade and conclude that annual EASAT will remain at current values or even slightly lower due to the weakening of the previous NAO in the case of little change in external forcing,

before resuming an upward trend over the following 10 years based on recent NAO decadal strengthening.

It is worth noting that this work only discussed the relationship between NAO and EASAT based on two cycles of data. These can be further verified based on paleoclimate proxy and climate model integration in the future. Also, some previous studies (Si et al. 2016; Yun and Timmermann 2018) have also suggested that as a quasi-white noise process, atmosphere itself varies at various time scales. Therefore, the mechanism of EASAT change might be further improved in the future. Furthermore, the model developed to predict annual EASAT does not consider the possible impact of volcanic eruptions and solar activity. In future work, we will further develop the prediction model, and improve its multidecadal prediction skill and apply it to more studies.

Acknowledgements This work was jointly supported by the National Key R&D Program of China (2016YFA0601801) and National Natural Science Foundation of China (NSFC) Project (41790474). The authors wish to thank all data providers and two reviewers for their constructive suggestions.

References

Allan RJ, Ansell TJ (2006) A new globally complete monthly historical mean sea level pressure data set (hadslp2): 1850–2004. J Clim 19(22):5816

Bradley RS, Diaz HF, Kiladis GN, Eischeid JK (1987) ENSO signal in continental temperature and precipitation records. Nature 327(6122):497–501

Bueh C, Shi N, Xie Z (2011) Large-scale circulation anomalies associated with persistent low temperature over southern China in January 2008. Atmos Sci Lett 12:273–280

Cess RD, Goldenberg SD (1981) The effect of ocean heat capacity upon global warming due to increasing atmospheric carbon dioxide. J Geophys Res Oceans 86(C1):498–502

Chen W, Yang S, Huang R (2005) Relationship between stationary planetary wave activity and the East Asian winter monsoon. J Geophys Res Atmos 110:D14

Compo et al (2011) The twentieth century reanalysis project. Q J R Meteorol Soc 137:1–28

Ding YH, Ren GY, Shi GY, Gong P, Zheng XH, Zhai PM, Zhang RH, Zhao ZC, Wang SW, Wang HJ, Luo Y, Chen DL, Gao XJ, Dai XS (2007) China's national assessment report on climate change (I): climate change in China and the future trend. Adv Clim Change Res 3:1–5

Gao LH, Yan ZW, Quan XW (2015) Observed and SST-forced multidecadal variability in global land surface air temperature. Clim Dyn 44(1–2):359–369

Gong DY, Wang SW, Zhu JH (2001) East Asian winter monsoon and arctic oscillation. Geophys Res Lett 28(10):2073–2076

Guan Z, Yamagata T (2003) The unusual summer of 1994 in East Asia: IOD teleconnections. Geophys Res Lett 30(10):235–250

Hansen J, Sato M, Ruedy R, Lo K, Lea DW, Medina-Elizade M (2006) Global temperature change. Proc Natl Acad Sci India 103(39):14288–14293

Hansen J, Ruedy R, Sato M, Lo K (2010) Global surface temperature change. Rev Geophys 48:RG4004

Hilmer M, Jung T (2000) Evidence for a recent change in the link between the North Atlantic oscillation and Arctic sea ice export. Geophys Res Lett 27(7):989–992

Hoskins BJ (1993) Rossby wave propagation on a realistic longitudinally varying flow. J Atmos Sci 50(12):1661–1671

Hu ZZ. Wu Z (2004) The intensification and shift of the annual North Atlantic oscillation in a global warming scenario simulation. Tellus 56(2):112–124

Hu ZZ, Jha B, Wang W, Huang B, Huang B (2012) An analysis of warm pool and cold tongue El Niños: air–sea coupling processes, global influences, and recent trends. Clim Dyn 38:2017–2035

Hua LJ, Ma ZG, Guo WD (2008) The impact of urbanization on air temperature across China. Theor Appl Climatol 93(3–4):179–194

Hunt BG, Wells NC (1979) An assessment of the possible future climatic impact of carbon dioxide increases based on a coupled one-dimensional atmospheric–oceanic model. J Geophys Res 84:787–790

Hurrell JW (1995) Decadal trends in the North Atlantic oscillation: regional temperatures and precipitation. Science 269(5224):676

Hurrell JW (1996) Influence of variations in extratropical wintertime teleconnections on Northern Hemisphere temperature. Geophys Res Lett 23(6):665–668

Hurrell JW, Kushnir Y, Ottersen G, Visbeck M (2003) An overview of the North Atlantic Oscillation. In: Hurrell JW, Kushnir Y, Ottersen G, Visbeck M (eds) The North Atlantic Oscillation: climatic significance and environmental impact. Geophysical monograph series, vol 134. American Geophysical Union, Washington, DC, pp 1–35

Kucharski F, Parvin A, Rodriguezfonseca B, Farneti R, Martinrey M, Polo I et al (2016) The teleconnection of the tropical Atlantic to Indo-Pacific sea surface temperatures on inter-annual to centennial time scales: a review of recent findings. Atmosphere 7(2):29

Levitus S, Antonov JI, Wang J, Delworth TL, Dixon KW, Broccoli AJ (2001) Anthropogenic warming of Earth's climate system. Science 292:267–270

Li YJ, Li JP (2012) Propagation of planetary waves in the horizonal non-uniform basic flow. Chin J Geophys 55:361–371 **(in Chinese)**

Li JP, Ruan CQ (2018) The North Atlantic–Eurasian teleconnection in summer and its effects on Eurasian climates. Environ Res Lett 13:024007

Li JP, Wang JXL (2003) A new North Atlantic oscillation index and its variability. Adv Atmos Sci 20(5):661–676

Li JP, Sun C, Jin FF (2013) NAO implicated as a predictor of Northern Hemisphere mean temperature multidecadal variability. Geophys Res Lett 40(20):5497–5502

Li YJ, Li JP, Jin FF, Zhao S (2015) Interhemispheric propagation of stationary Rossby waves in the horizontally nonuniform background flow. J Atmos Sci 72:3233–3256. https://doi.org/10.1175/JAS-D-14-0239.1

Li C, Zhao T, Ying K (2016) Effects of anthropogenic aerosols on temperature changes in China during the twentieth century based on CMIP5 models. Theor Appl Climatol 125(3–4):529–540

Li JP, Sun C, Ding RQ (2018a) A coupled decadal-scale air–sea interaction theory: the NAO-AMO-AMOC coupled mode and its impacts. In: Beer T, Li JP (eds) Global change and future earth—the geoscience perspective. Cambridge University Press, Alverson, pp 131–143

Li JP, Hsu HH, Wang WC et al (2018b) East Asian climate under global warming: understanding and projection. Clim Dyn. https://doi.org/10.1007/s00382-018-4523-6

Lin Y, Franzke CLE (2015) Scale-dependency of the global mean surface temperature trend and its implication for the recent hiatus of global warming. Sci Rep 5:12971

Liu Q, Wen N, Liu Z (2006) An observational study of the impact of the North Pacific SST on the atmosphere. Geophys Res Lett 33(18):273–274

Luo FF, Li SL (2014) Joint statistical–dynamical approach to decadal prediction of East Asian surface air temperature. Sci China Earth Sci 57:3062–3072
Luterbacher J, Schmutz C, Gyalistras D, Xoplaki E, Wanner H (1999) Reconstruction of monthly NAO and EU indices back to AD 1675. Geophys Res Lett 26(17):2745–2748
Meehl GA, Teng H (2014) CMIP5 multi-model hindcasts for the mid-1970 s shift and early 2000s hiatus and predictions for 2016–2035. Geophys Res Lett 41(5):1711–1716
Meehl GA, Teng H, Arblaster JM (2014) Climate model simulations of the observed early-2000 s hiatus of global warming. Nat Clim Change 4(10):898–902
Morice CP, Kennedy JJ, Rayner NA, Jones PD (2012) Quantifying uncertainties in global and regional temperature change using an ensemble of observational estimates: the HadCRUT4 dataset. J Geophys Res 117:D08101
Peng S (2002) Mechanism for the NAO response to the North Atlantic SST tripole. J Clim 16(12):1987–2004
Polyakov IV, Johnson MA (2000) Arctic decadal and interdecadal variability. Geophys Res Lett 27(24):4097–4100
Pyper BJ, Peterman RM (1998) Comparison of methods to account for autocorrelation in correlation analyses of fish data. Can J Fish Aquat Sci 55:2127–2140
Robeson SM, Willmott CJ, Jones PD (2014) Trends in hemispheric warm and cold anomalies. Geophys Res Lett 41:9065–9071
Scaife AA, Knight JR, Vallis GK, Folland CK (2005) A stratospheric influence on the winter NAO and North Atlantic surface climate. Geophys Res Lett 32(18):109–127
Schlesinger ME (1994) An oscillation in the global climate system of period 65–70 years. Nature 367(6465):723–726
Si D, Hu ZZ, Kumar A, Jha B, Peng P, Wang W, Han R (2016) Is the interdecadal variation of the summer rainfall over eastern China associated with SST? Clim Dyn 46(1–2):135–146
Slonosky V, Yiou P (2002) Does the NAO index represent zonal flow? the influence of the NAO on North Atlantic surface temperature. Clim Dyn 19(1):17–30
Stocker T, Qin D, Plattner GK, Tignor M, Allen SK, Boschung J, Nauels A, Xia Y, Bex V, Midgley PM (2014) Climate change 2013: the physical science basis. Cambridge University Press, Cambridge
Stolpe MB, Medhaug I, Knutti R (2017) Contribution of Atlantic and Pacific multidecadal variability to twentieth-century temperature changes. J Clim 30(16):6279–6295
Stolpe MB, Medhaug I, Sedláček J, Knutti R (2018) Multidecadal variability in global surface temperatures related to the Atlantic Meridional Overturning Circulation. J Clim 31(7):2889–2906
Sun YB, Clemens SC, Morrill C (2012) Influence of Atlantic meridional overturning circulation on the East Asian winter monsoon. Nat Geosci 5:46–49
Sun C, Li JP, Jin FF (2015) A delayed oscillator model for the quasi-periodic multidecadal variability of the NAO. Clim Dyn 45:1–17
Sun C, Li JP, Ding RQ, Jin Z (2017) Cold season Africa–Asia multi-decadal teleconnection pattern and its relation to the Atlantic multidecadal variability. Clim Dyn 48:11–12
Sun C, Li JP, Kucharski F, Xue JQ, Li X (2018) Contrasting spatial structures of Atlantic multidecadal oscillation between observations and slab ocean model simulations. Clim Dyn 51. https://doi.org/10.1007/s00382-018-4201-8
Taylor KE, Stouffer RJ, Meehl GA (2012) An Overview of CMIP5 and the experiment design. Bull Am Meteorol Soc 93(4):485–498
Thompson SL, Schneider SH (1979) A seasonal zonal energy balance climate model with an interactive lower layer. J Geophys Res 84:2401–2414
Trenberth KE, Paolino DA J (1980) The Northern Hemisphere sea-level pressure data set: trends, errors and discontinuities. Mon Wea Rev 108(7):855–872
University of East Anglia Climatic Research Unit; Harris IC, Jones PD CRU TS4.01 (2017) Climatic research unit (CRU) time-series (TS) version 4.01 of high-resolution gridded data of month-by-month variation in climate (Jan. 1901–Dec. 2016). Centre for Environmental Data Analysis
Walker GT (1924) Correlations in seasonal variations of weather IX. Mem Indian Meteor Dept 24:275–332
Wallace JM, Gutzler D (1981) Teleconnections in the geopotential height field during the Northern Hemisphere winter. Mon Wea Rev 109(4):784–812
Wang L, Chen W (2014) A CMIP5 multimodel projection of future temperature, precipitation, and climatological drought in China. Int J Climatol 34(6):2059–2078
Wang XF, Li JP, Sun C, Liu T (2017) NAO and its relationship with the Northern Hemisphere mean surface temperature in CMIP5 simulations. J Geophys Res Atmos 122(8):4202–4227
Wanner H, Bronnimann S, Casty C, Gyalistras D, Luterbacher J, Schmutz C, Stephenson DB, Xoplaki E (2001) North Atlantic oscillation-concepts and studies. Sur Geophys 22(4):321–382
WCRP (World Climate Research Program) (2018) CLIVAR Initial implementation plan. WCRP
Wu B, Wang J (2002) Winter arctic oscillation, siberian high and East Asian winter monsoon. Geophys Res Lett 29(19):1–3
Yang T, Tao Y, Li J, Zhu Q, Su L, He X, Zhang X (2017) Multi-criterion model ensemble of CMIP5 surface air temperature over China. Theor Appl Climatol 6:1–16
Yoshino MM (1978) Climate change and food production. University of Tokyo, Tokyo, p 331
Yu B, Lin H, Wu ZW, Merryfield WJ (2016) Relationship between North American winter temperature and large-scale atmospheric circulation anomalies and its decadal variation. Environ Res Lett 11:074001
Yun KS, Timmermann A (2018) Decadal monsoon-ENSO relationships re-examined. Geophys Res Lett 45(4):2014–2021
Zhang JC, Liu ZG (1992) Climate of China. P376
Zhao P, Jones P, Cao L, Yan Z, Zha S, Zhu Y, Yu Y, Tang G (2014) Trend of surface air temperature in Eastern China and associated large-scale climate variability over the last 100 years. J Clim 27(12):4693–4703
Zhao S, Li JP, Li YJ (2015) Dynamics of an interhemispheric teleconnection across the critical latitude through a southerly duct during boreal winter. J Clim 28:7437–7456. https://doi.org/10.1175/JCLI-D-14-00425.1
Zhao S, Li JP, Li YJ, Jin FF, Zheng JY (2018) Interhemispheric influence of Indo-Pacific convection oscillation on Southern Hemisphere rainfall through southward propagation of Rossby waves. Clim Dyn. https://doi.org/10.1007/s00382-018-4324-y
Zhou L, Dickinson RE, Tian Y, Fang J, Li Q, Kaufmann RK (2004) Evidence for a significant urbanization effect on climate in China. Proc Natl Acad Sci USA 101:9540–9544
Zuo J, Ren HL, Li W (2015) Contrasting impacts of the Arctic oscillation on surface air temperature anomalies in southern China between early and middle-to-late winter. J Clim 28(10):4015–4026